

Metal-Organic Frameworks derived Hollow polyhedron Metal Oxide Posited Graphene oxide for Energy Storage Applications

Bendi Ramaraju*, Cheng-Hung Li, Sengodu Prakash and Chia-Chun Chen*

Department of Chemistry, National Taiwan Normal University, Taipei 116, Taiwan.

E-mail: ramarajubendi@gmail.com; cjchen@ntnu.edu.tw

Preparation of GO: Few-layered graphene oxide was prepared using the modified Hummers method from the graphite. Briefly, two grams of graphite and 1.5 g of NaNO₃ (A.R.) were placed in a flask. Then, 60 mL of H₂SO₄ (A.R.) was added with stirring in an ice-water bath, and 9.0 g of KMnO₄ (A.R.) was slowly added over about 1h. The stirring was continued for 2h in the ice-water bath and then it was continually stirred for 5d at room temperature. Then, 6 mL of H₂O₂ (30 wt%) was added in the suspension, and the mixture was stirred for 2h at room temperature. Then wash the substance with aqueous solution (1L H₂O+ 31.2g. H₂SO₄ + 14.3g H₂O₂) several times, and then the sample was rinsed with deionised water until the solution was neutral. The desired products were dried in a vacuum oven at room temperature. Formation of GO was confirmed by Raman (Fig. S1), IR and XRD (Fig. S2).

Preparation of MOF: In a typical procedure, 5g. copper nitrate (Cu(NO₃)₂·3H₂O) and 2.5g. benzene-1,3,5-tricarboxylic acid (C₆H₃(COOH)₃) were dissolved in a methanol under ultrasonication, respectively. After that, the copper nitrate solution was transferred into the tricarboxylic acid solution. The mixture solution was kept at room temperature for 2h until MOF precipitation finished. The precipitation was retrieved by centrifugation and washed with methanol for two times. At last, the blue powder of [Cu₃(btc)₂]_n was dried in vacuum at room temperature. The formation of [Cu₃(btc)₂]_n polyhedrons was confirmed by powder X-ray diffraction (PXRD) (Fig. S6), TEM and SEM (Fig. S7 and S8).

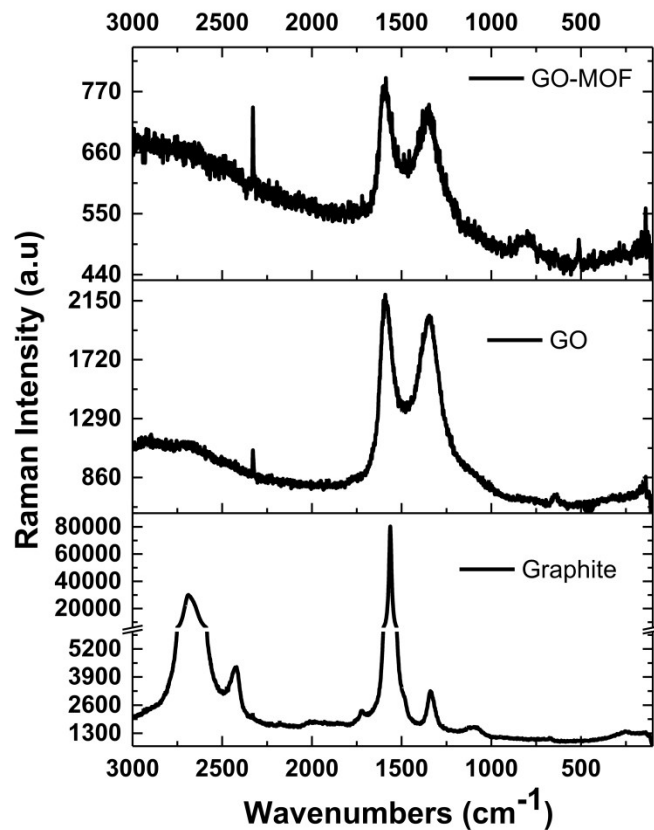


Fig. S1: Raman spectra of various carbon materials.

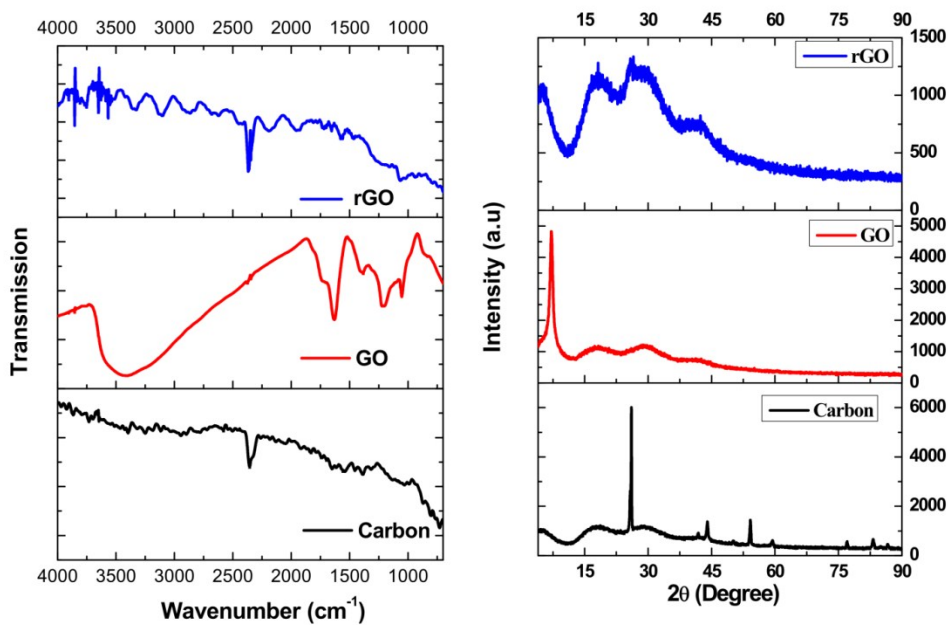


Fig. S2: IR and XRD spectra of various carbon materials.

Preparation of the rGO-CuO/Cu₂O hollow polyhedron: 1:1 weight ratio of GO and MOF were dispersed in methanol-water mixture and the resulting mixture was vigorously stirred for overnight at room temperature. The mixture was vacuum-dried at 80 °C for overnight. Thus as-prepared GO-MOF composite was transferred to a tube furnace. Before being heated, the furnace tube was flushed twice by high-purity nitrogen gas to remove oxygen. The furnace was then heated to 500 °C and maintained at this temperature for 60 min under nitrogen gas flow. After that, the temperature was reduce to 350 °C and then the nitrogen gas flowing was switched off and the furnace was still kept at this temperature for another 60 min in flowing air. Finally, the product was taken out and labelled as Cu_{ox}-rGO, further uses it for remaining characterizations and analysis. The systematic experimental procedure was shown in Fig. S3. Blank sample was prepared for comparison with same procedure using GO and Cu(NO₃)₂.3H₂O and named as GO-CuO blank.

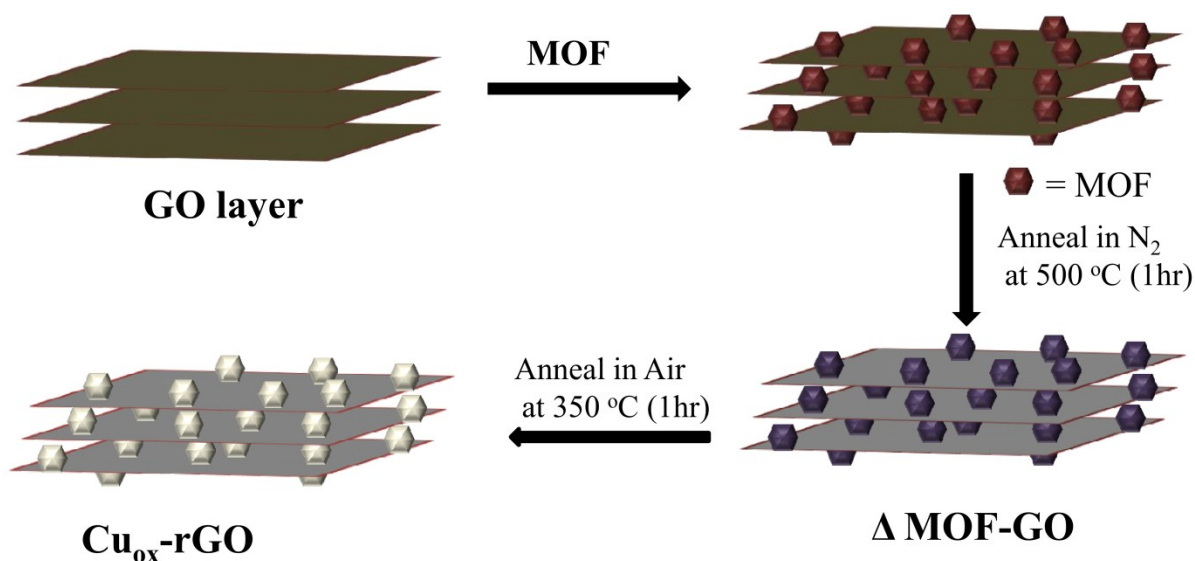


Fig. S3: Schematic illustration of the process used for the synthesis of Cu_{ox}-rGO composites.

Structure and morphology characterization:

Thermo gravimetric analysis (TGA) was recorded using a TA instrument Q500 under nitrogen/air flow at a heating rate of 10 °C/min. Raman spectrum was recorded by using inVia confocal Raman microscope. X-ray analysis was performed using a Bruker D8 Advanced diffractometer with Cu K α radiation at a wavelength of $\lambda = 0.154056$ Ao, operated at 40 kV and

30 mA. The morphology of the final products was characterized by scanning electron microscopy (SEM) (JEOL JSM-6510). Transmission electron microscopy(TEM) and corresponding high resolution TEM images were obtained by a Philips/FEI Tecnai 20 G2 s-Twin Transmission Electron Microscopy with an accelerating voltage of 100 kV. The samples were ultrasonically dispersed in ethanol and dropped onto the TEM grids, and allowed subsequent solvent evaporation in air at room temperature.

Electrochemical measurements:

The electrochemical behaviour of the MOF, GO, Cu_{ox}-rGO and CuO-GO composites was examined using CR2032 coin type cells. The working electrodes were prepared using a slurry coating procedure. A weight ratio of 55:25:20 of as synthesized composite, Super P carbon and poly(vinyl difluoride) (PVDF) dissolved in N-methylpyrrolidinone (NMP) were mixed together and stirred 3h to obtain a uniform slurry. The slurry was coated on a copper foil current collector and kept overnight in vacuum oven at 90 °C. The foil was compressed using stainless steel roller and cut into 16 mm diameter electrodes. Test cells were assembled in argon filled glove box and all the cells evaluated by galvanostatically discharge-charge cycled using a computer-controlled AcuTech Systems BAT-750B Battery Automatic Tester in between 0.005-3.0 V at different current densities. The measured values were normalized per gram of the active material. Cyclic voltammetry and Impedance measurements were performed on fresh coin cell samples using potentiostat/galvanostat (Autolab®PGSTAT-302N, Eco Chemie B.V., The Netherlands) using a voltage range of 0.005 to 3.0 at a scan rate of 0.5 mV s⁻¹.

Fabrication of lithium-ion battery:

A piece of metallic lithium (thickness, 0.59 mm, Kyokuto Metal Co., Japan) was used as the reference and counter electrodes, 1 M LiPF₆ in ethylene carbonate (EC)-dimethylcarbonate (DMC) (1:1 volume ratio) as the electrolyte and a glass micro-porous disk (Whatman) as the separator.

Fabrication of sodium-ion battery:

A piece of metallic sodium foil (0.3 mm thickness, Shimakyu's Pure Chemistry) was used as the counter electrode and Cu_{ox}-rGO electrode was used as the working electrode. The electrodes were electronically separated by GF/C Whatman (GE Healthcare UK limited) as the separator saturated with 1 M NaPF₆ in various solvents including ethylene carbonate and propylene carbonate (EC: PC = 1:1, v/v) as the electrolyte.

Figure S4 represents the Raman spectra of the MOF, Cu_{ox}-rGO and GO. Raman spectrum of Cu_{ox}-rGO not only preserved the major characteristic peaks of the MOF, but also exhibited G and D bands of GO. In the Raman spectrum of GO, the characteristic G and D bands were observed at 1593 cm⁻¹ and 1352 cm⁻¹, respectively. The G band was usually assigned to the E_{2g} phonon of C sp² atoms, while the D band was a breathing mode of κ-point phonons of A_{1g} symmetry. The Raman spectrum of the MOF exhibited characteristic bands at 744 cm⁻¹ corresponding to out-of-plane ring bending vibrations and to out-of-plane ring (C-H) bending modes; 1609 and 1006 cm⁻¹ are associated with (C=C) stretching modes of benzene ring and the signals at 1463 and 1551 cm⁻¹ corresponding to symmetric and asymmetric stretching of the carboxylate units.^{1,2}

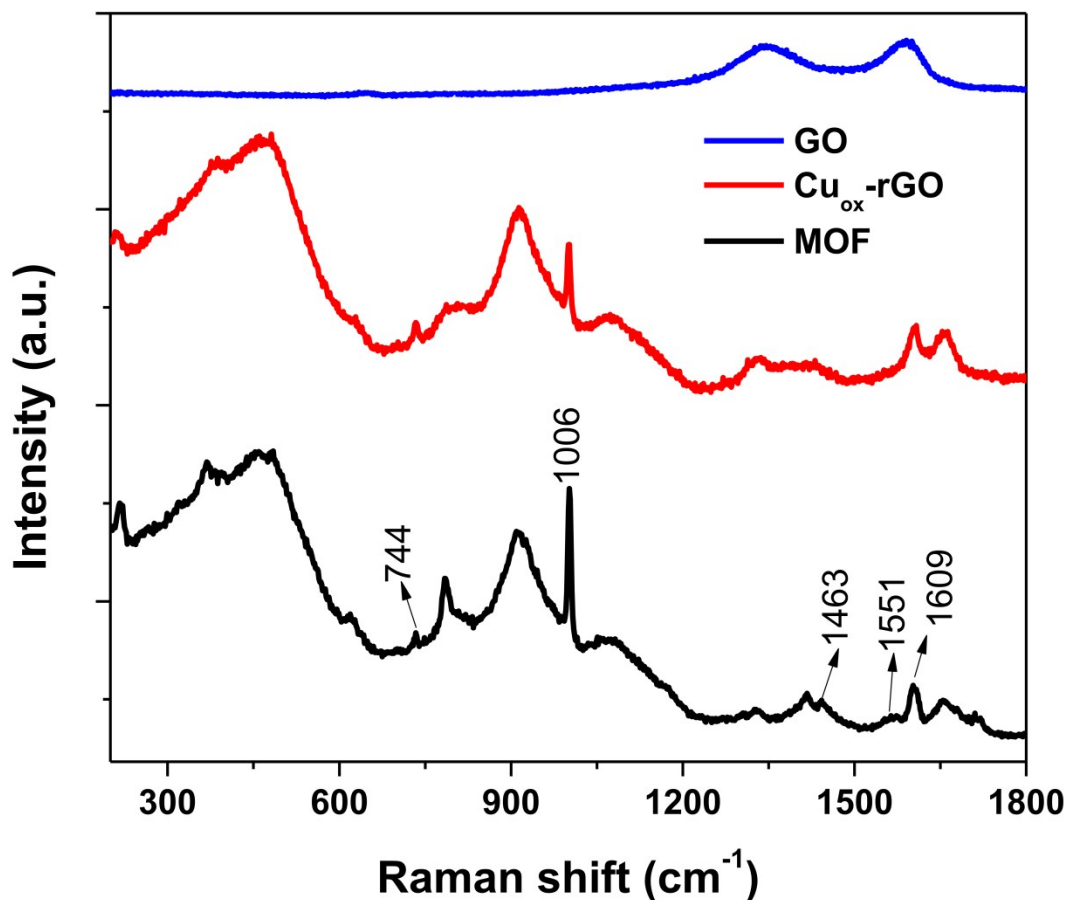


Figure S4. Raman spectra of various materials.

The thermal stability and the thermal behavior of various samples were investigated through TGA. Figure S5 shows the TGA curves of MOF, GO-MOF and GO samples for 25 -700 °C under N₂ gas (Fig. S5A) and Δ MOF, Δ MOF-GO and Δ GO (“ Δ ” the samples heated at 500 °C under N₂ atmosphere) samples under air (Fig. S5B). Two steps of weight loss were noted (Fig. S5a) for GO and MOF samples and the GO-MOF composite exhibit three different types of weight loss. The first step of weight loss from 40–130 °C for GO (~27% weight loss), 200–250 °C temperature ranges for MOF (~7% weight loss) and the first two steps of weight loss in GO-MOF composite (~20%) are attributed to the loss of physically and chemically adsorbed water, respectively. Further mass loss around 200-350 °C for GO (~60% weight loss) and 300-450 °C for MOF (~80% weight loss) and GO-MOF (~65% weight loss) was due to decomposition of residual oxygen-containing functional groups(mainly epoxy and hydroxyl groups). As can be observed, the weight loss of the GO in the removal of residual oxygen functional groups process is much lower than that of the MOF and GO-MOF. Fig. S5B shows the weight loss at 300, 480 and 560 °C for Δ MOF, Δ MOF-GO and Δ GO, respectively in presence of air due to decomposition carbon skeleton of the organic ligands and GO.

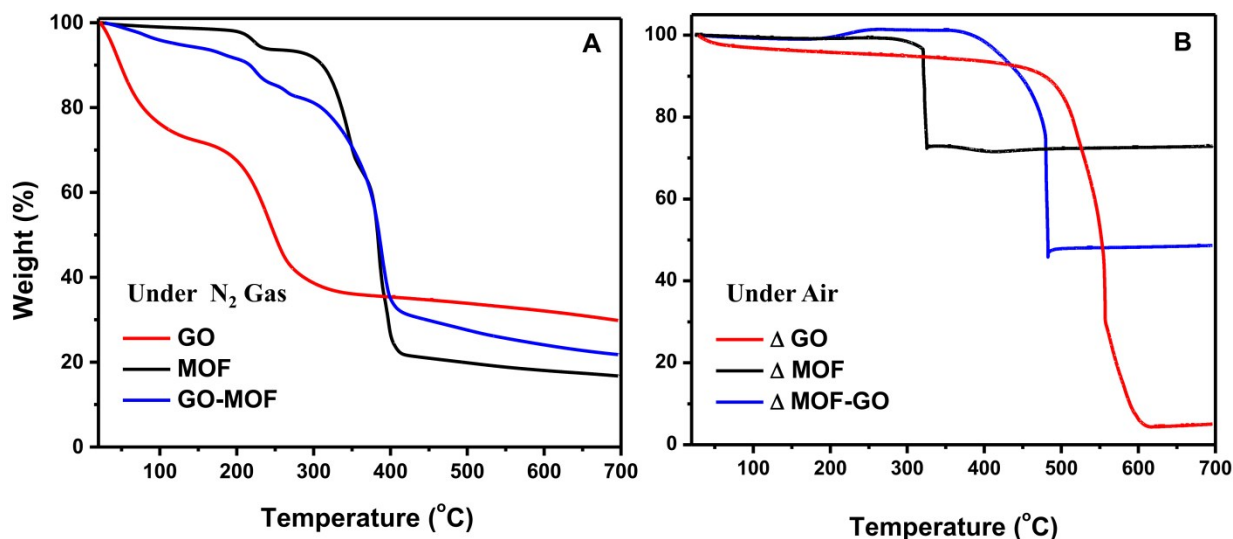


Figure S5. TGA curves of various materials.

The powder XRD was used to check the structural identity and phase transition of the samples. It can be expected that the addition of graphene will create a high density of grain boundaries due to its presence in the crystal. As shown in Fig.S6, the GO-MOF's XRD peak

positions are in well agreement with the parent MOF crystal, which means that the unit cell of the parent MOF is maintained. After calcination under N_2 gas, decomposition of the crystal structure of MOF and formation of metal oxide was observed. At final product, Cu_{ox} -rGO composite exhibits diffraction peaks at 2θ values of 32.2, 35.07, 38.3, 48.07, 53.04, 57.81, 61.08, 67.75 and 74.63, which are assigned to the (110), (002), (111), (-202), (020), (220), (220) and (311) planes of monoclinic CuO , and also 36.03, 42.35, 61.08, 65.66 and 72.15 peaks were assigned to the (111), (200), (220), (221) and (311) planes of Cu_2O , respectively.³ All these observations indicate that the final samples were successfully prepared with Cu_{ox} on reduced graphene oxide by the use of MOF as a precursor by heat treatment.

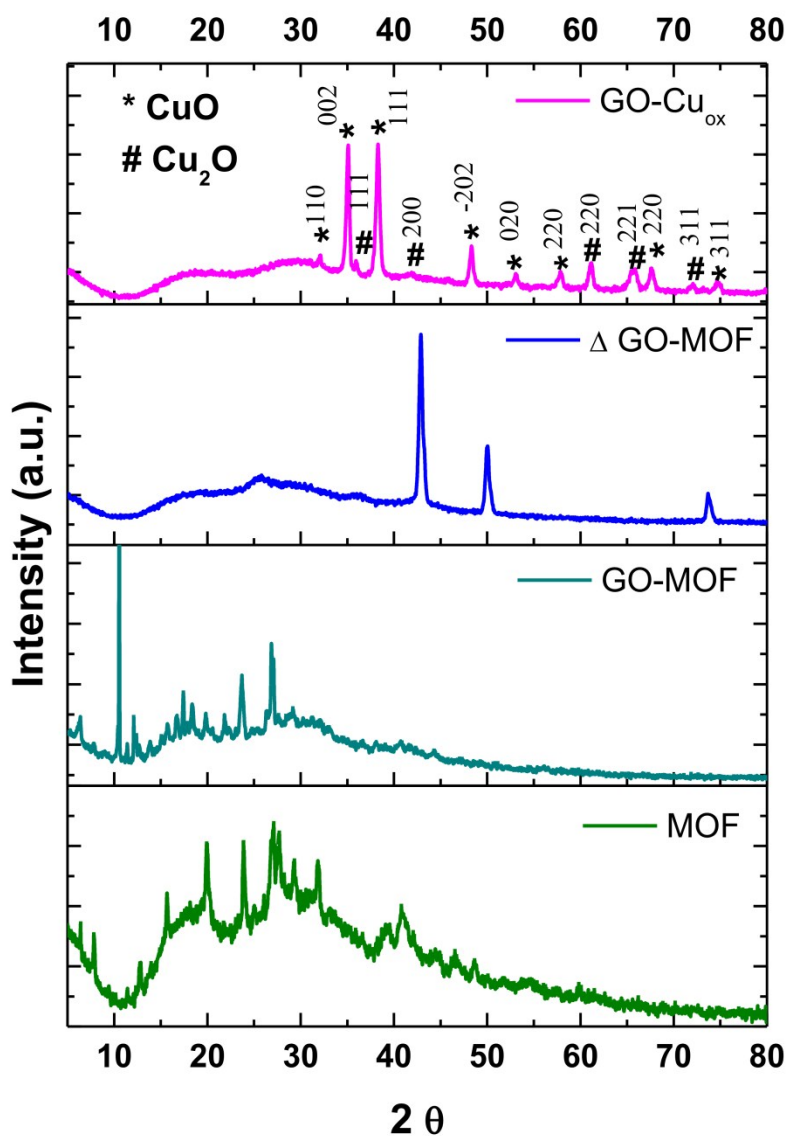


Figure S6. X-Ray diffraction patterns of various materials.

In Figure S7, the morphology of the microstructure of MOF and Cu_{ox} -rGO were studied by using TEM and SEM. From the TEM images of Cu_{ox} -rGO, it can be observed that all the Cu_{ox} particles are firmly attached to the graphene oxide sheets even after the ultrasonication used to disperse the Cu_{ox} -rGO composite for TEM characterization. We can find that the sizes of most Cu_{ox} NPs anchored on graphene oxide are in the range of 200-500 nm. A few Cu_{ox} NPs agglomeration on the GO sheet was observed in Cu_{ox} -rGO TEM image (Fig. S8). The morphology of the MOF crystal and Cu_{ox} -rGO composites were also examined using SEM. The SEM image of pure MOF (Right panel of the Fig. S7 shows that the MOF crystals are octahedron shape with micron sized crystals. Cu_{ox} -rGO composite shows a strong interaction between graphene sheet and Cu_{ox} particles.

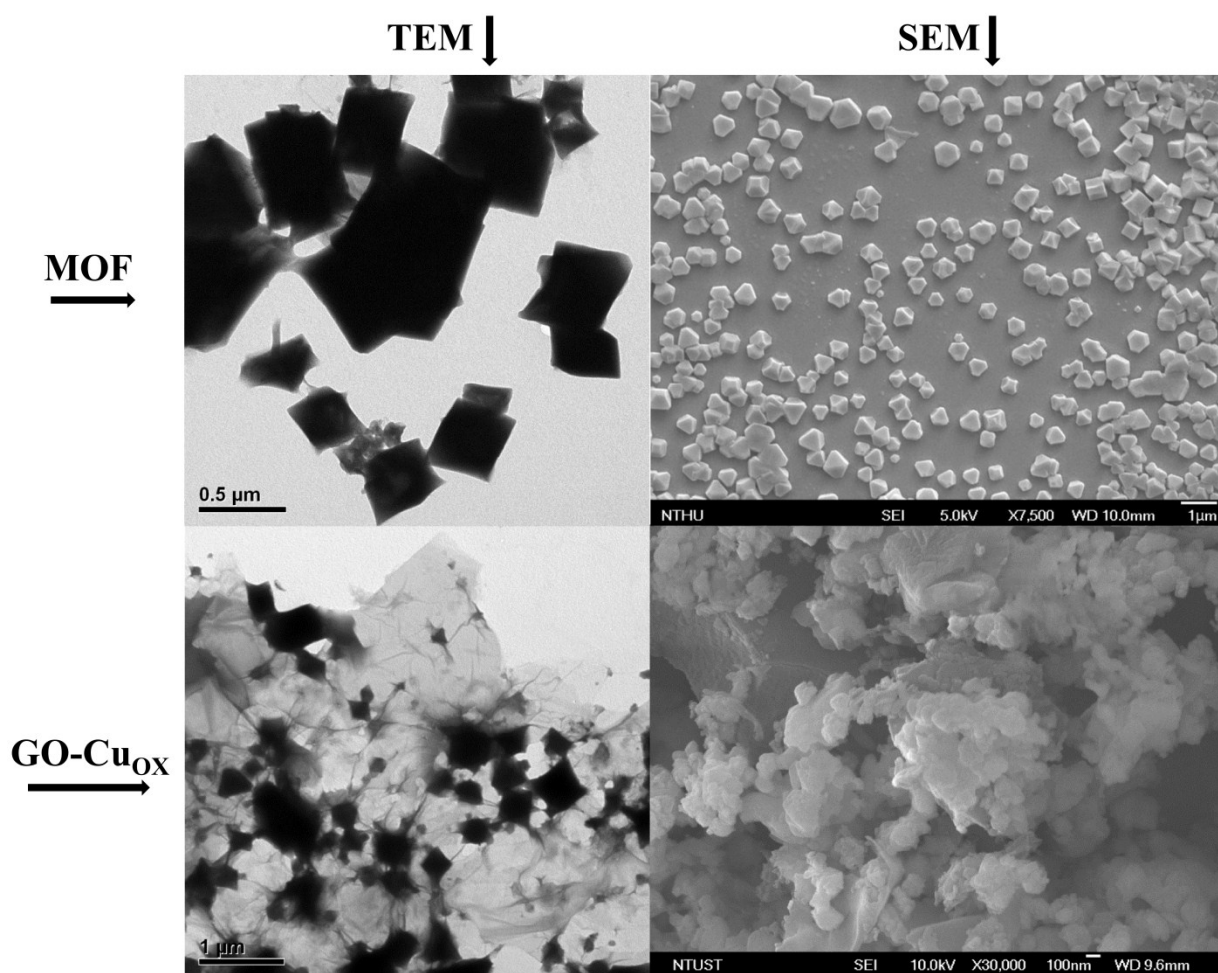


Figure S7. SEM and TEM images of MOF and Cu_{ox} -rGO composite.

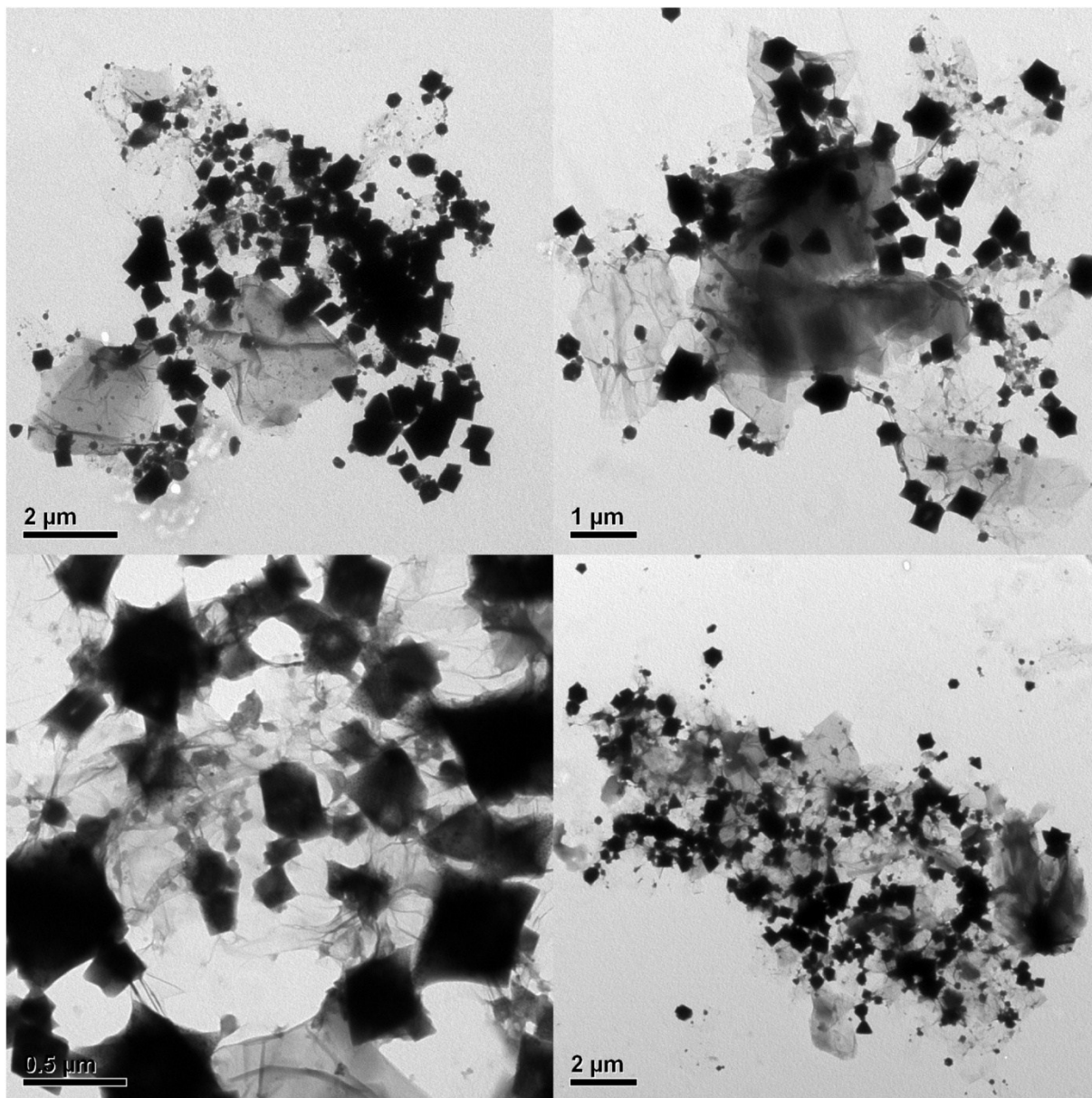


Fig. S8: TEM images of Cu_{ox} -rGO composite

The chemical states of the compositional elements in Cu_{ox} -rGO composite was revealed by the XPS and the representative spectra of Cu_{ox} -rGO composite is shown in Fig. S9. Figure S9 (A), the survey spectrum, the indexed peaks are only correspond to elements C, N, O and Cu. The main peaks of carbon (C1s, 284.4 eV), nitrogen (N1s, 399.5 eV), oxygen (O1s, 532.5 eV). More details about the chemical form in which copper is present can be inferred from the detail spectra shown in Figure S9 (B). The XPS spectra of the core levels of the Cu 2p were analyzed to estimate the copper oxidation state. The Cu 2p_{3/2} and 2p_{1/2} peaks formed doublets by peak fitting suggesting that the chemical state is mainly Cu^{1+} and Cu^{2+} . the binding energy of 934.2 eV for the Cu 2p_{3/2} and 954.3 eV for the Cu 2p_{1/2} peaks were the characteristic of Cu^{2+} species, while lower binding energy of 932.1 eV and 952.1 eV was the characteristic of Cu^{+} .^{4,5}

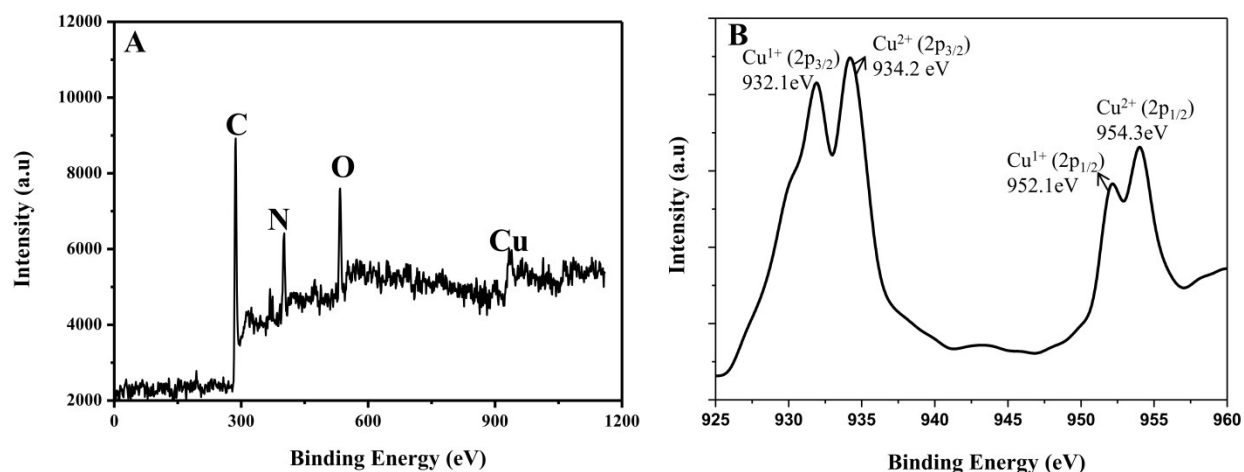


Fig. S8: XPS analysis of Cu_{ox} -rGO composite (A) Survey spectrum; B) Detailed spectrum of Cu

The modeling of EIS spectra for MOF and Cu_{ox} -rGO modified electrodes' surface was done using Randles electrical equivalent circuit (Figure S9) which consist of a solution resistance R_s connected in series with the SEI film capacitance and resistance, C_f and R_f (elements in parallel to each other) and in series with the double layer capacitance C_{dl} , charge transfer resistance, R_{CT} and Warburg impedance (Z_w) related to the diffusion of lithium ions into the electrodes, respectively. The diameter of the semicircle increases with the intercalation of lithium ion, indicating that the film and contact resistances increase steadily. Whereas the charge transfer resistance is due to electron transfer generated by the redox probes present in the electrolyte solution. By calculation, (Table S1) it is also found that the R_{CT} values of Cu_{ox} -rGO is lesser than

pure MOF, GO and CuO-rGO blank electrodes. It is also observed that the continuous decrease of apparent charge transfer resistance in Cu_{ox}-rGO while increasing the number of cycles which proves a continuous improvement of electron transfer kinetics and, simultaneously, charges accumulation. Overall, the electrochemical properties of Cu_{ox}-rGO have revealed a complex and interesting behavior which makes them great candidates for fabrication of energy storage devices

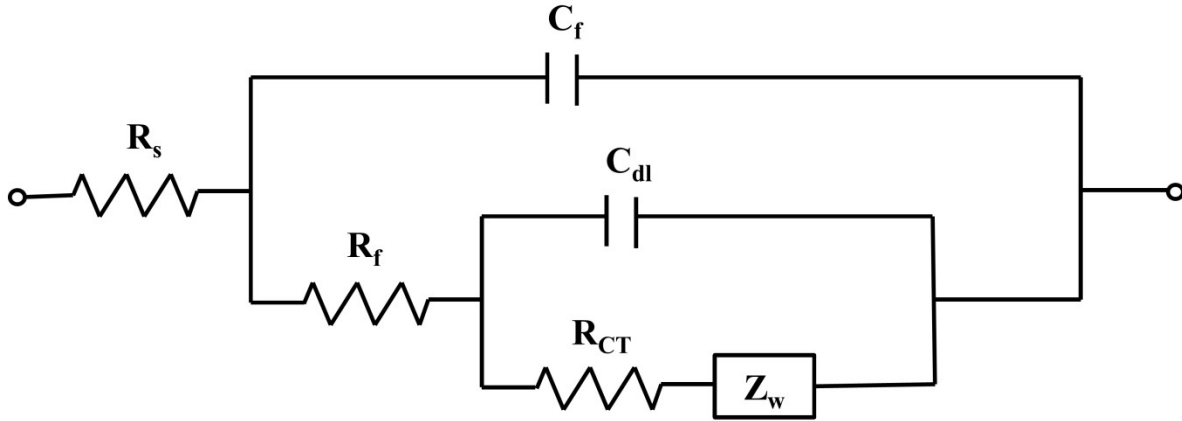


Fig. S10: Randles equivalent circuit

Table S1: Parameters values obtained from fittings of the impedance spectra represented in Figure 2

EIS plot	$R_s(\Omega)$	$R_f(\Omega)$	$R_{CT}(\Omega)$
MOF	6.44	600	968
GO	10.85	-	397
GO-CuO Blank	7.91	243	325
Cu _{ox} -rGO before cycle	7.33	114	166
Cu _{ox} -rGO after 1 st cycle	4.11	115	191
Cu _{ox} -rGO after 15 th cycle	4.43	132	260
Cu _{ox} -rGO after 50 th cycle	6.43	116	234
Cu _{ox} -rGO after 100 th cycle	4.65	-	97
Cu _{ox} -rGO after 150 th cycle	5.20	-	72
Cu _{ox} -rGO after 200 th cycle	7.91	-	48
Cu _{ox} -rGO after 250 th cycle	7.17	-	37
Cu _{ox} -rGO after 300 th cycle	8.92	-	31

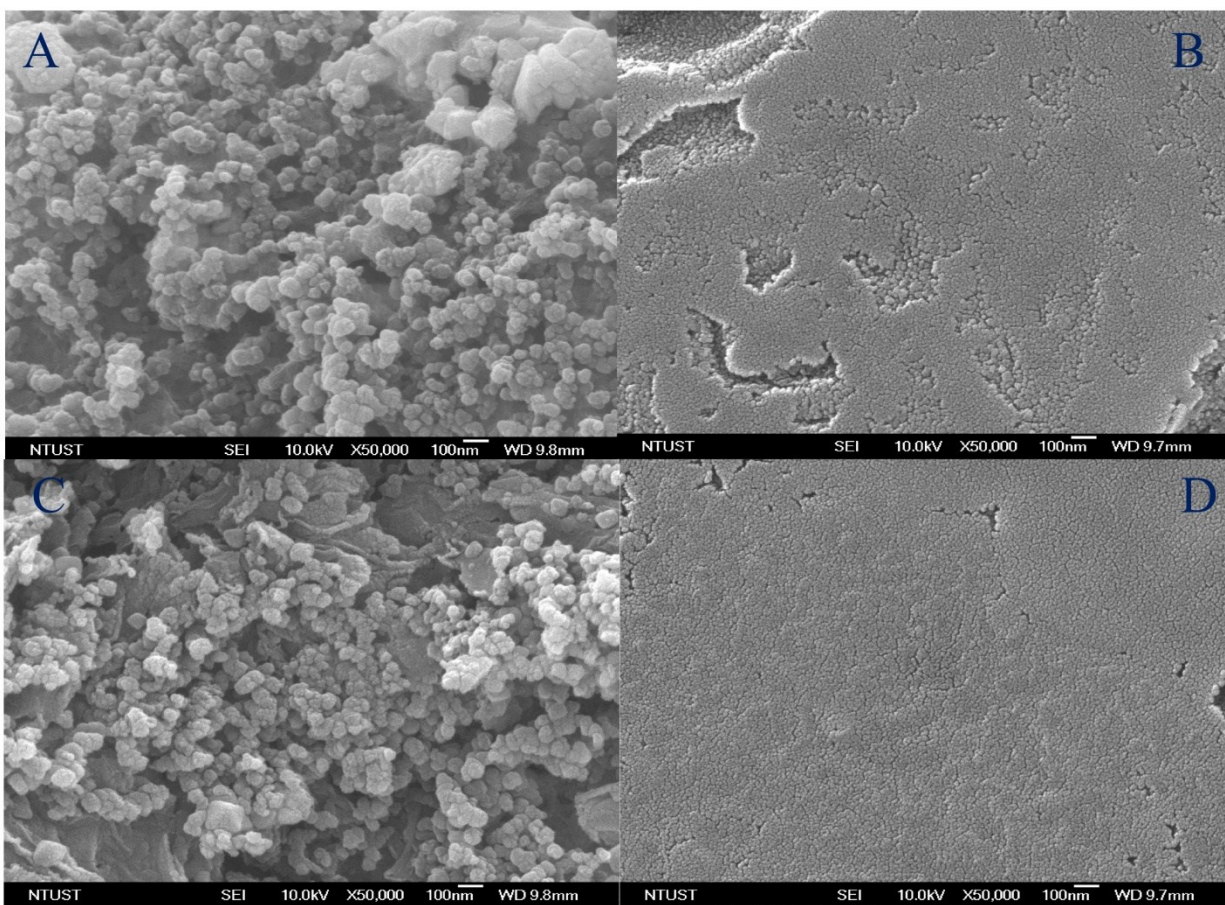


Fig. S11: A&C) SEM images of Cu_{ox}-rGO electrodes before cycles, B&D) SEM images of Cu_{ox}-rGO electrodes after 500 cycles at 1000 mA. g⁻¹,

References:

- 1 C. Prestipino, L. Regli, J.G. Vitillo, F. Bonino, A. Damin, C. Lamberti, A. Zecchina, P.L. Solari, K.O. Kongshaug and S. Bordiga, *Chem. Mater.*, 2006, **18**, 1337.
- 2 E. Biemmi, A. Darga, N. Stock and T. Bein, *Micropor. Mesopor. Mat.*, 2008, **114**, 380-386.
- 3 L. Hu, Y. Huang, F. Zhang and Q. Chen, *Nanoscale*, 2013, **5**, 4186-4190.
- 4 M. Biesinger, L. Lau, A. Gerson and R. Smart, *Appl. Surf. Sci.*, 2010, **257**, 887–898.
- 5 B. Ramaraju and T. Imae, *RSC Adv.*, 2013, **3**, 16279–16282.